Bull. Chem. Soc. Ethiop. **2024**, 38(3), 563-576.
DOI: https://dx.doi.org/10.4314/bcse.v38i3.2

ISSN 1011-3924
Printed in Ethiopia
Online ISSN 1726-801X

# WAX SCREEN-BASED FABRICATION OF PAPER DEVICES FOR THE DETERMINATION OF IRON IN PARTICULATES OF SELECTED WELDING FUMES IN ADDIS ABABA, ETHIOPIA

Gizachew Wendimu[1], Ahmed Hussen[1*] and Raj Mohan B.[2]

[1]Center for Environmental Science, College of Natural and Computational Sciences, Addis Ababa University, P. O. Box 1176, Addis Ababa, Ethiopia
[2]Department of Chemical Engineering, National Institute of Technology Karnataka, Surathkal, India

(Received November 21, 2023; Revised February 17, 2024; Accepted February 19, 2024)

**ABSTRACT**. In this study a paper-based analytical device was developed using screen printing technique for the determination of particulate iron from welding fumes. The operational parameters such as volume and concentration of 1,10-phenanthroline, volume and concentration of hydroxylamine were optimized by the Box Behnken Design (BBD) using Minitab. Additionally, the μ-PAD's sample solution holding capacity and reaction time were also optimized. Under the optimized condition, particulate metal concentrations were colorimetrically quantified using a handheld mobile phone and image processing software, ImageJ. Very good analytical performance such as good linearity of the calibration curve and better selectivity was observed by the developed method. The limit of detection for $Fe^{3+}$ assay was 4.6 mg/L; which is adequate to determine the threshold concentration limit of particulate iron set by the regulatory bodies (6 mg/L). The μ-PAD revealed 95-99% recovery compared with the UV-Vis spectrophotometry (98-100%). Furthermore, welding fume samples were collected in Addis Ababa over five days, using mixed cellulose ester filters and the findings show a high concentration that exceeds the standard levels. Analyzing particulate iron with μ-PADs yielded results consistent with UV-Vis spectrophotometry, suggesting μ-PADs' potential application for occupational particulate iron exposure measurement, eliminating the need for expensive analytical devices.

**KEY WORDS**: μ-PADs, Particulate iron, Response surface methodology, Wax screen-printing, Welding fume, Colorimetric detection

## INTRODUCTION

Particulate metals are among the potent pollutants to humans and its environs as they are non-biodegradable and can accumulate in ecological systems. Apart from their natural existence, metallic aerosols could be released into the environment by both natural and anthropogenic sources [1]. These particulates are known to be toxic and carcinogenic, thus contributing mainly to the development of lung cancer [2-4], pneumoconiosis [5, 6], respiratory impairment and cardiovascular disease [7-9] and metal fume fever [10-12].

Particulate iron (Fe) has been selected for this study, since it accounts for the highest proportion of the metal particulates found in welding fumes [13]. The Occupational safety and health administration (OSHA) has set the workplace exposure limit of iron oxide (measured as Fe) to be 14 mg/m$^3$ (6 mg/L) [14], and the Ethiopian Environmental Protection Authority (EPA) limit values for emissions to air in production and processing of iron and steel is 10 mg/L. According to the Addis Ababa city government's labor enterprise and industry development bureau, there are now roughly 1691 firms operating in the welding sector. These welding workplaces are scattered around the city, near residential and commercial areas, increasing the risk of contamination to the rest of the neighborhood. Despite the risks posed by the inhalation of these hazardous metal particulates, assessment of welders' exposure is very limited in developing nations due to unaffordability of the conventional analytical instruments such as Inductively

*Corresponding author. E-mail: ahmed.hussen29@aau.edu.et

Coupled Plasma-Atomic Emission Spectrometry (ICP-AES), Isotope Dilution/Inductively Coupled Plasma Mass Spectrometry (ID/ICP-MS) and Photometric. The conventional instruments are expensive, needs time-consuming sample pre-treatment and skilled personnel for operation. The demand for environmental and worker's safety analysis in an affordable approach necessitates the exploration for sensitive and rapid determination methods for particulate metals [15-21].

Microfluidic paper-based analytical device (μ-PAD) is a device involving manipulation of microliter volumes of a sample through capillary action directed along defined flow paths in a fibrous network, with or without the assistance of reagents or added energy. Subsequent to fabrication, colorimetric methods are primarily employed for the quantification of the analyte, owing to their simplicity and compatibility with cost-effective reporting systems such as smartphones. μ-PADs possess competitive advantages over conventional analytical instruments, such as being inexpensive, portability and simplicity. They are also identified as point-of-care devices and successfully applied in several fields such as diagnostics, biological, food safety, environmental monitoring and biotechnology [22-29].

Several studies have employed μ-PADs for the detection of iron in environmental samples such as water, welding fume standards, incineration ash, dust and natural hot spring. The majority of the studies reported a high limit of detection (LOD) in the range of 12-20 mg/L. All of the reported LODs fail to meet the permissible limits set by various regulatory bodies such as OSHA and EPA. This suggests that the sensitivity of the reported μ-PADs is insufficient to predict the threshold concentration that could cause an environmental threat [30-34].

Thus, in this work we are reporting a μ-PAD system with an improved analytical sensitivity to meet the OSHA and EPA's permissible exposure limit (PEL). Unlike previously reported analysis techniques, we incorporate two pretreatment zones which helps to remove interferences more effectively than a single pretreatment zone and improve the device's sensitivity for particulate iron analysis by improving the selectivity and masking capacity of the preloaded reagents [35]. Furthermore, the effect from surrounding light to the image capturing was controlled by using smart phone in-built free application called OpenCamera. And also, a Multivariate approach which was rarely employed in the previous studies has been used for optimization of experimental parameters in the development of μ-PAD.

## EXPERIMENTAL

### *Chemicals and Reagents*

Iron(III) chloride hexahydrate (97%), 1,10-phenanthroline (99%), methyl orange, sodium acetate trihydrate (99%), cadmium(II) nitrate tetrahydrate (98%) and zinc(II) nitrate hexahydrate (98%) were purchased from Sigma-Aldrich. Nickel(II) sulfate hexahydrate (Alfa Aesar, 98%), glacial acetic acid (Fisher Scientific, 95%), Nitric acid (EMD Millipore, 65%), Fotolack TR-88 and diazo F sensitizer (Feteks), sodium bicarbonate (99.7%) and sodium acetate (99%) (UNI-CHEM) were used to carry out the experiments. All chemicals used were of analytical grade and used as received without further purification. Aqueous solutions were prepared using deionized (DI) water, which was obtained from a water purification system (EXL 3, Vivagen, Korea).

### *Apparatus*

Spectral measurements were carried out using a UV-Vis spectrophotometer (HACH DR600). OMAX light microscope and electronic balance were used to examine the hydrophilic/hydrophobic region and for weight measurement, respectively. Intermediate air sampling pump (SKC 224-PCTX4 Model, SKC Ltd), Whatman No. 1 qualitative grade filter paper, mixed cellulose ester (MCE) filter (0.8 μm, Ø 25 mm) (Fisher Scientific), micropipettes

0.1–2.5, 10–100, 100–1000 µL (Eppendorf, Germany), Nikai microwave oven (1000 W, NMO2309MW), Samsung galaxy A30 phone, Hairdryer (2000 watts), wooden frame (20 cm x 30 cm), Nylon mesh (75 micron), solid candle-making wax, squeegee and adhesive tape were purchased from local market.

*Device design and fabrication*

A wax screen-printing method reported by Tesfaye and Hussen [36] has been used with some modifications, such as using ecofriendly A4 paper instead of plastic films. The fabrication process can be categorized into three phases: i) printing the design of interest on A4 paper ii) transferring the pattern to the mesh and iii) fabricating the µ-PAD. Each phase involves a series of steps as illustrated in Figure 1A. The design of interest was sketched using Microsoft PowerPoint 2019 and printed on A4 paper using a laser printer. Black areas on the paper are used to create a hydrophobic area on the filter paper, while white areas yield hydrophilic zones (Figure1A (Ia)).

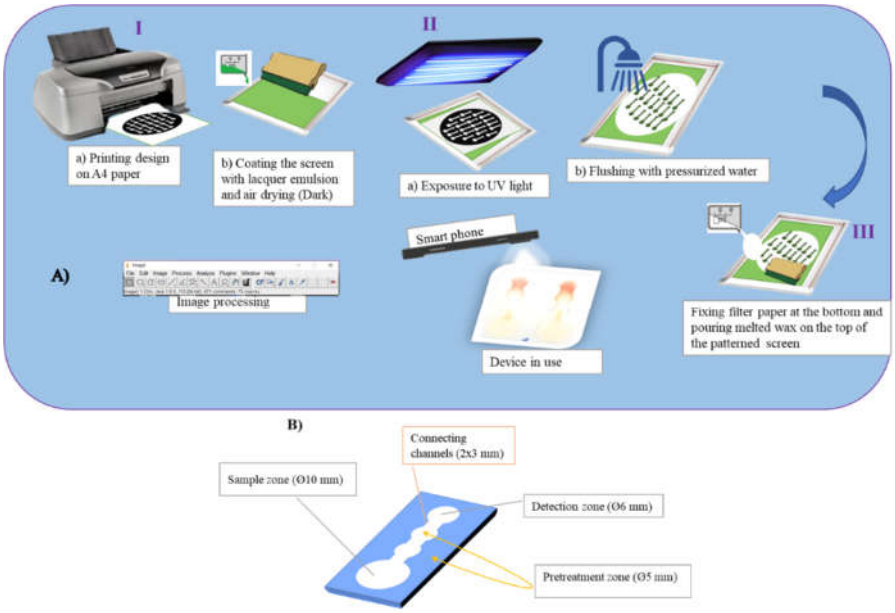


Figure 1. A) µ-PAD fabricated by wax screen printing on Whatman filter paper, grade 1. B) µ-PAD with the dimensions of each zone.

A fine mesh of size 75 micron was stretched on a 20x30 cm wooden frame. A lacquer emulsion was prepared by mixing FOTOLACK CH88 photo emulsion with diazo F sensitizer (9:1) and left overnight in a dark area. The emulsion was applied on both sides of the mesh and dried in a dark box to keep away from light exposure (Figure 1A (Ib)). After drying, the printed A4 paper was placed over the coated-screen and then exposed to a UV-light source (2500 lux) at a distance of 30 cm (Figure 1A (IIa)). The light passes through the white areas and creates a polymerization (hardening) of the emulsion directly on the coated mesh. The area of coated-screen that is exposed to light becomes tough which will create a hydrophilic part on the filter paper, preventing the percolation of the wax applied later on, while the unexposed area could easily be flashed with pressurized water opening the mesh for creating the hydrophobic part on the filter paper (Figure

1A (IIb)). In due course, to fabricate the μ-PAD, a Whatman No. 1 qualitative grade filter paper was put on the bottom of the patterned screen and pre-melted candle-making wax was poured on to the patterned screen from the top and squeegeed to insert the melted wax into the screen (Figure 1A (III)). The wax printed paper was made ready for use after removing the paper from the mesh using a household hair drier (2000 watts). It was allowed to cool to room temperature followed by sealing the backside of the device with clear packing tape to prevent the leakage of the fluid through the flow channel during analysis. As shown in Figure 1B, the fabricated μ-PAD has separate zones with defined dimensions.

*Optimization of operation parameters*

In response surface methodology (RSM), a MINITAB 2021 software was used for the experimental design, determination of the coefficients, data analysis, and graph plotting. The mathematical model was developed and established to get a functional relationship between independent variables and the response. An empirical second-order polynomial model (Eq. 1) was utilized to characterize the effect of variables in terms of linear, quadratic, and interaction terms with in the mathematical model.

$$Y = b_o + \sum_{i=1}^{k} b_i \mathrm{x}_i + \sum_{i=1}^{k} b_{ii} x_i^2 + \sum_{i<j}^{k} b_{ij} \mathrm{x}_i \mathrm{x}_j + \cdots + e \quad (1)$$

where, Y is response variable, $b_0$, $b_i$, $b_{ii}$ and $b_{ij}$ are the constant coefficient, linear coefficient, quadratic coefficient and the interactive coefficients, respectively and *e* represents the random error.

The statistical significance of the developed model and terms were evaluated by analysis of variance (ANOVA). The quality of the model was determined by the coefficients of determination ($R^2$). The significance of the model terms was determined according to the p-value and a 95% of confidence level. The contour plots with its corresponding surface plots were constructed to estimate the relationship between the independent variables and response (intensity) [37].

The operation parameters such as concentration of 1,10-phenanthroline (4–20 mg/mL), volume of phenanthroline (0.1–1.5 μL), concentration of hydroxylamine (0.05-0.2 g/mL) and volume of hydroxylamine (0.1-1.5 μL) were optimized in the range indicated by RSM using the Box Behnken Design (BBD). Subsequently, the reaction time (60-240 sec) was evaluated by measuring the color intensity formed at the detection zones at different time interval. Moreover, the holding capacity (volume) of the device was optimized by using 2 mM of methyl orange indicator solution.

*Colorimetric detection*

After optimizing the operational parameters, a solution of an acetate buffer (6.3 M, pH 4.5) for the Fe assay was prepared by using sodium acetate trihydrate (15 g) and glacial acetic acid (11.75 mL) in 50 mL of water. Both 1,10-phenanthroline (20 mg/mL) and hydroxylamine (0.05 g/mL) were prepared as separate solutions, each in the acetate buffer. The μ-PAD was prepared for detection of Fe by first adding the optimum volume (0.1 μL) of hydroxylamine solution to each pretreatment zones followed by 1.5 μL aliquots of 1,10-phenanthroline to the detection reservoir. The device was allowed to dry completely between each addition of reagent and finally 15 μL aliquot of sample solution containing analyte of interest was added to form an orange colored ferroin complex $[Fe(phen)_3]^{2+}$ as shown in scheme 1 [32].

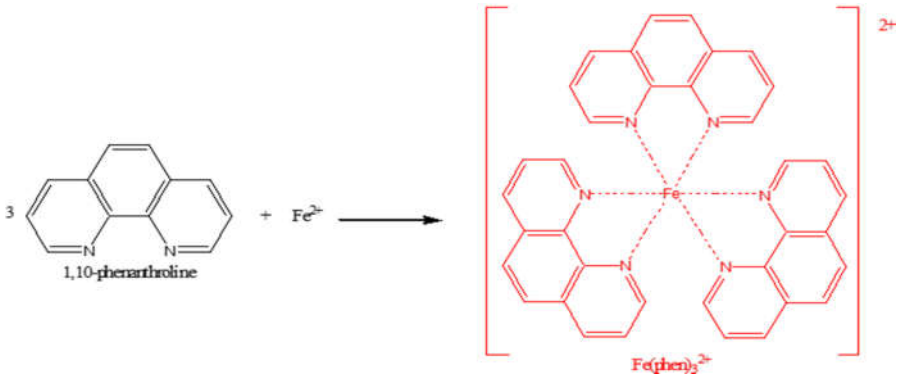


Scheme 1. Reaction of $Fe^{2+}$ with 1,10-phenanthroline.

The color developed was captured using a Samsung galaxy A30 smartphone in-built free application OpenCamera, fixing the camera settings as ISO value (100), Exposure (Locked), Camera Flash (Off), Exposure compensation (+1EV) and Zoom (x2). A smartphone's built-in application system reduces the impact of ambient light variation on intensity, encouraging on-site use of the device. Finally, the corresponding color intensity was analyzed as mean grayscale intensity using ImageJ software.

*Real sample collection, digestion and analysis*

Real samples were obtained from metal arc welding workplaces located at Gurara (site 1) and Akaki kaliti (site 2) in the city of Addis Ababa where the metal arc welding technology is being widely used.

The US Occupational Safety and Health Administration's sampling approach, an air sample taken near an individual's breathing zone over the course of an eight-hour shift, was employed [38]. As a result, a person-carried device (Figure 2) called the Intermediate air sampling pump (SKC 224-PCTX4 Model, SKC Ltd, UK) was used, with the sampling unit consisting of a portable Institute of Occupational Medicine (IOM) multi fraction dust sampler. The air flow rate was set to 4 L/min, which is widely used for personal exposure assessment since it approximates the average human breath rate as mentioned by Mentele *et al.* [32]. The pump was slung around the welder's waist, and the inlet cyclone (IOM) was hooked to the collar as close to the breathing zone of the welder as possible.

Samples were taken on multiple days in the vicinity of each welding operation. Aerosol was sampled onto 25 mm mixed cellulose ester (MCE) filters (0.8 µm pore size) and sampling duration lasts approximately eight hours. After sample collection, 10 mm punches were taken from each filter using biopsy punch and subjected to household microwave-assisted acid digestion [32] by adding 5 µL of concentrated nitric acid, followed by 30 µL of water to the filter punches. After that, the punches were placed in a domestic microwave oven on high power for 45 s. Every 15 s, the process was stopped, and an additional 30 µL of water was added to punches to stimulate further digestion. Finally, 8 µL of sodium bicarbonate (0.5 M) was added to neutralize the acid on the filter punches, which were then analyzed under the optimal conditions of the developed colorimetric µ-PAD system.

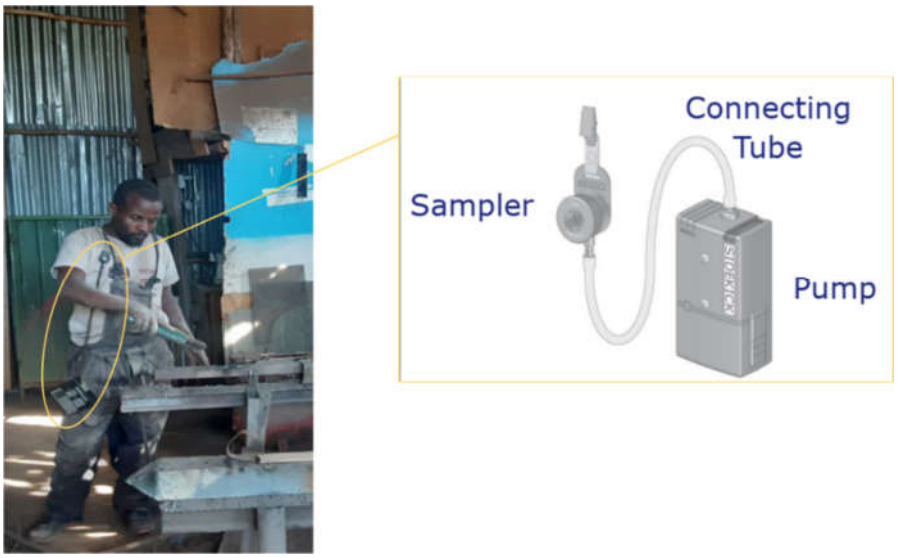


Figure 2. Sampling technique for particulate metal collection.

## RESULTS AND DISCUSSION

*Characterization of printed microfluidic channels in the paper surface*

The surface of the filter paper was modified using molten candle wax. And the digital microscopy was used to examine the surface changes that occur on the cellulose fibers after modification.

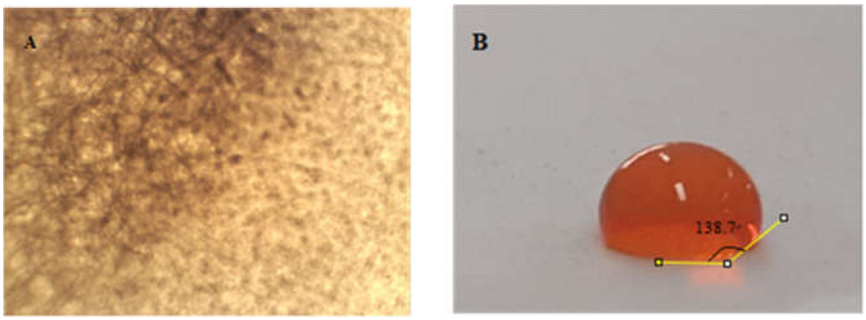


Figure 3. A) The hydrophilic and hydrophobic barrier of the device using digital microscope image (40X) B) Water contact angle (WCA) measurement.

The digital microscope image result (Figure 3A), clearly shows the permeability of the paper to hold the loaded reagents with in the given flow channel. However, on the hydrophobic region (light region) the porous part of the cellulose was blocked by the wax creating the patterned paper of interest which directs the flow of the reagents through the proper channel. Another evidence for the efficient formation of the hydrophobic barrier comes from contact angle measurement.

The measurement of the contact angle formed by a droplet of liquid placed on a horizontal surface, the so-called sessile drop, is one of the most used methods to study the surface properties. It is an easy and quick method that can be used to evaluate the homogeneity of the coating, surface cleanliness and adhesion. If the solid surface is hydrophobic, the contact angle would be greater than 90°, and surfaces with a contact angle greater than 150° are known to be super-hydrophobic [39, 40]. As it can be seen from Figure 3B, the surface of a candle-making wax modified filter paper showed a contact angle of 138.7°. This clearly demonstrates that the hydrophobic wax penetrates throughout the thickness of the filter paper and able to effectively guide the flow of the aqueous solution within the hydrophilic region. Similar result (contact angle of 129° ) has been reported in a recent work by Tesfaye and Hussen [36].

*Optimization of sample volume and reaction time*

The sample volume is the amount of reagent needed to spread onto the entire test region (hydrophilic part) to complete colorimetric reaction. Figure 4 shows the holding capacity of the μ-PADs for the sample volume obtained after a few seconds of stay using 2 mM methyl orange solution. The trials showed that the optimum drop volume should fall on 15 μL. This maximum holding capacity was taken into consideration while loading reagents and sample solution throughout the whole experiments.

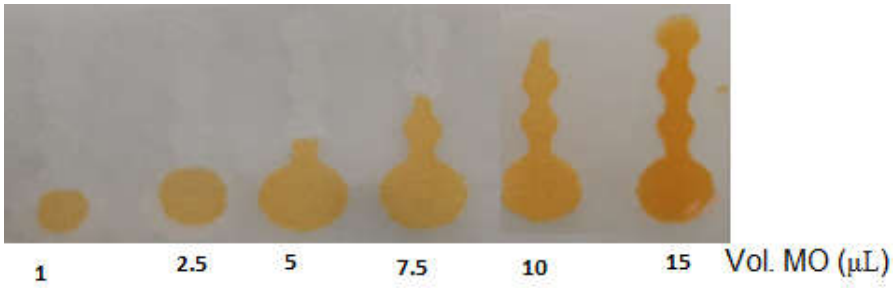


Figure 4. Optimization of fluid holding capacity of the designed μ-PAD using methyl orange (MO) indicator.

The reaction time for maximum color intensity was investigated by capturing the image developed at the detection zone. The intensity saturates beyond 90 s and therefore 120 s was considered as the best time for image acquisition.

*RSM optimization of operational parameters in μ-PADs*

The use of RSM was found to have several advantages over the one factor at time, such as the identification of interaction, the use of statistical analysis that produces model equations for optimization and prediction of a specific system's behavior. These upsides would absolutely help in minimizing the cost and time spent for the experiment by reducing the number of trials [41].

In this study a total of 27 experiments were designed and performed to optimize the effect of the individual independent variables (concentration of 1,10-phenanthroline, volume of 1,10-phenanthroline, concentration of hydroxylamine and volume of hydroxylamine) using BBD method. The complete experimental design was developed and a quadratic model was proposed to correlate the independent variables for maximum intensity output by using RSM.

Intensity = 49.45 - 0.053 A - 1.61 B + 194.7 C + 18.55 D + 0.0594 A*A + 18.29 B*B + 881 C*C- 2.41 D*D + 2.210 A*B - 18.98 A*C + 0.129 A*D - 164.6 B*C - 29.23 B*D + 43.3 C*D

where A-concentration of 1-10 phenanthroline, B-volume of 1,10-phenanthroline, C-concentration of hydroxylamine and D-volume of hydroxylamine.

The reliability of the proposed model was verified using coefficients of determination ($R^2$), the percent of the variation of the response explained by the model. It is also a measure of fit, i.e. how well the model fits the data [42]. The results of the analysis of variance (ANOVA) and lack-of-fit (LOF) tests as generated from the experimental data are shown in Table 1. A higher F-value indicates that the regression equation can explain the majority of the variables in the response, and probability values less than 0.05 are considered statistically significant. Hence, from the regression model summary results, the values of $R^2$ and adjusted-$R^2$ are close to 1 revealing a high degree of correlation between the observed and predicted values of the hue intensity. This could also imply that the proposed quadratic model equation provides the foreseen levels of accuracy [43, 44]. Furthermore, the insignificant lack of fit ($p = 1.81 > 0.05$) depicts that the quadratic model is suitable for predicting the response and adequately fits the experimental data. The linear, quadratic, and interaction effects of the studied parameters also reveals that the linear effect of all parameters have negative significance, except the volume of hydroxylamine has positive significant effect. The quadratic and 2-way interaction effects of all the studied variables have negative significant effects on the color intensity except the interaction between the concentration of 1,10-phenanthroline/volume of hydroxylamine and concentration of hydroxylamine/volume of hydroxylamine.

Table 1. ANOVA of the developed model for the μ-PAD analysis.

| Source | DF | Adj SS | Adj MS | F-value | p-value |
|---|---|---|---|---|---|
| Model | 14 | 4635.54 | 331.110 | 32.25 | 0.000 |
| Linear | 4 | 1760.43 | 440.108 | 42.86 | 0.000 |
| A | 1 | 581.72 | 581.717 | 56.65 | 0.000 |
| B | 1 | 612.47 | 612.469 | 59.65 | 0.000 |
| C | 1 | 548.51 | 548.506 | 53.42 | 0.000 |
| D | 1 | 17.74 | 17.739 | 1.73 | 0.213 |
| Square | 4 | 601.23 | 150.307 | 14.64 | 0.000 |
| A*A | 1 | 77.03 | 77.030 | 7.50 | 0.018 |
| B*B | 1 | 428.45 | 428.447 | 41.72 | 0.000 |
| C*C | 1 | 130.97 | 130.966 | 12.75 | 0.004 |
| D*D | 1 | 7.45 | 7.452 | 0.73 | 0.411 |
| 2-Way interaction | 6 | 2273.88 | 378.979 | 36.91 | 0.000 |
| A*B | 1 | 612.56 | 612.563 | 59.65 | 0.000 |
| A*C | 1 | 518.93 | 518.928 | 50.54 | 0.000 |
| A*D | 1 | 2.09 | 2.088 | 0.20 | 0.660 |
| B*C | 1 | 298.77 | 298.771 | 29.10 | 0.000 |
| B*D | 1 | 820.82 | 820.823 | 79.94 | 0.000 |
| C*D | 1 | 20.70 | 20.703 | 2.02 | 0.181 |
| Error | 12 | 123.22 | 10.269 | | |
| Lack-of-fit | 10 | 110.95 | 11.095 | 1.81 | 0.408 |
| Pure error | 2 | 12.27 | 6.135 | | |
| Total | 26 | 4758.76 | | | |

The response optimization of the independent variables revealed that as the values of A and B approach the maximum, the intensity increases, while the values of C and D become sufficient to achieve the maximum intensity with the minimum amount. As a result, the optimal values, for variables A, B, C, and D are found to be 20 mg/mL, 1.5 μL, 0.05 g/mL, and 0.1 L, respectively.

Similarly, the contour plot of individual variables and the surface plot (Figure5) illustrate that the highest intensity was achieved at high concentration (A) and volume (B) of the chromophore whereas the effect of the concentration (C) and volume (D) of reducing agent looks enough at minimal values. The result obtained from both plots showed that the interaction was mainly dependent on the chromophore concentration and volume where as there is no need of excess volume of the reducing/masking agent.

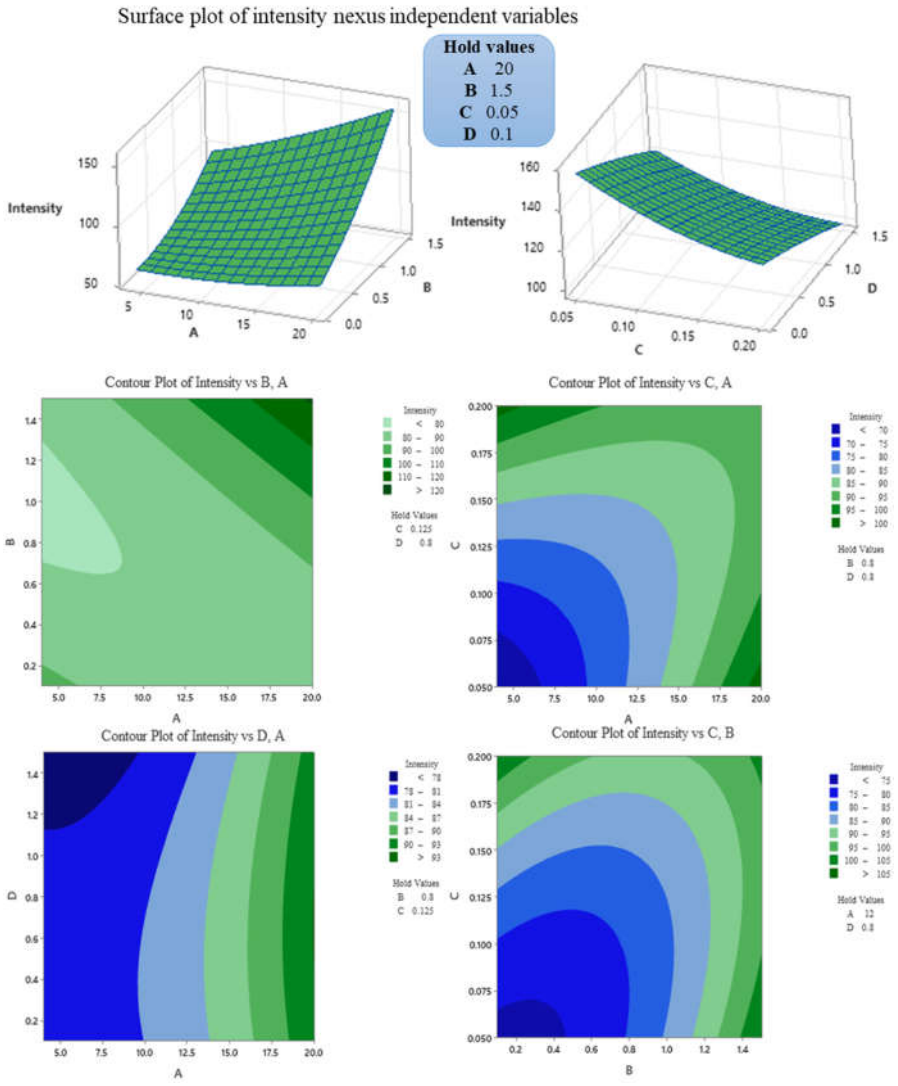


Figure 5. The response surface plot and response contour plot of the effects of parameters A (concentration of 1,10-phenanthroline), B (volume of 1,10-phenanthroline), C (concentration of hydroxylamine) and D (volume of hydroxylamine).

*Analytical performance of the method*

*Calibration curves*

The calibration curve was constructed using a standard solution of $Fe^{3+}$ in the concentration range of 0.1 to 50 mg/L under pre-optimized conditions. The calibration curve obtained using µ-PADs has a good linearity with a correlation coefficient $R^2$-value of 0.993 whereas using UV-Visible spectrophotometry the $R^2 = 0.999$.

*Limit of Detection*

In both µPADs and UV-vis, the detection limit was determined based on the international committee on harmonization (ICH) of analytical techniques which recommends to estimate the LOD and LOQ from standard deviation of the response and slope of the calibration curve obtained from the Excel regression output [45]. In µ-PAD analysis the limit of detection (LOD) and limit of quantification (LOQ) for $Fe^{3+}$ assay was found to be 4.6 and 15.2 mg/L, respectively. In the case of UV-Vis, LOD and LOQ was 0.32 and 0.97 mg/L, respectively. Although µ-PADs are less sensitive compared with UV-Vis, the result indicates the potential applicability of the µ-PADs for the point-of-need purpose since its LOD is below the regulatory limits set by OSHA or EPA.

Table 2. Comparison with previously reported µ-PADs for the determination of iron.

| Target metal ion | LOD (mg/L) | Complexing agent | Reference |
|---|---|---|---|
| Fe(III) | 15 | 1,10-Phenanthroline | Rattanarat, et al. [34] |
| Fe(III) | 20 | 4,7-Diphenyl-1-1, 10-phenanthroline | Cate, et al. [31] |
| Fe(III) | 12 | 1,10-Phenanthroline (phen) monohydrate | Ogawa and Kaneta [33] |
| Fe(III) | 15 | 1,10-Phenanthroline | Mentele, et al. [32] |
| Fe(III) | 0.64 | 1,10-Phenanthroline monohydrate | Asano and Shiraishi [30] |
| Fe(III) | 4.6 | 1,10-Phenanthroline | This study |

The data in Table 2 indicates that the limit of detection (LOD) for iron assay in this study (4.6 mg/L) demonstrates greater sensitivity compared to previously published findings. [31-34]. In contrast, Asano and Shiraishi [30] revealed a lower LOD by utilizing a paper device with test spots where no diffusion occurred due to the usage of a single spot reservoir. In general, the present study demonstrates that the developed µ-PAD analysis of iron has suitable sensitivity to evaluate compliance with the PEL of iron (10 mg/L) in working areas set by the Ethiopian EPA without need for the conventional analytical instrument/approach [18].

*Interference study*

As shown in Figure 6, the result demonstrates there is a negligible effect from the coexisting ions at a concentration level of 1:1 and 1:2 ratio of iron to other metal ions (Cd, Ni and Zn). This is because 1,10-phenanthroline hardly form complexes with those ions; instead it prefers to form stable complex with iron [30]. Additionally, in this study two pretreatment zone design was employed which enhances the masking of the coexisting metals and improve the sensitivity. Likewise, the application of two pretreatment zone for other metal assay was investigated by kamnoet *et al.* [35] and similar effects were reported.

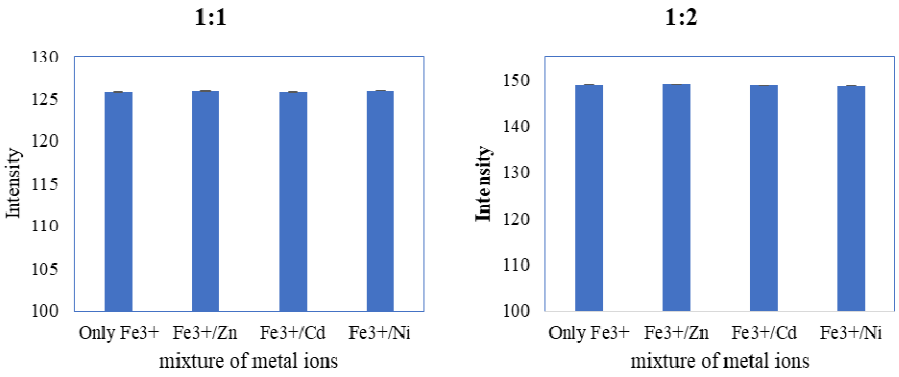


Figure 6. Interference study of coexisting ions.

*Method validation*

The proposed μ-PAD was applied for the determination of spiked $Fe^{3+}$ in aqueous solution and the assay results were compared to those obtained by UV-Vis spectrophotometer. Various concentration levels were spiked in aqueous solution and determined using the fabricated μ-PADs and a UV-Visible spectrophotometer. The percentage recovery observed for $Fe^{3+}$ was 95-99 and 98-100% by using μ-PADs and UV-Visible spectrophotometry, respectively. The μ-PAD method result is in a very good agreement with UV-Visible spectrophotometry and therefore it could also be used for the basic assay of $Fe^{3+}$ in a resource-limited area without a need for an expensive and complicated analytical technique.

*Real sample analysis and air quality status in the welding area*

The samples were collected, digested and analyzed with the μ-PAD and parallelly with the UV-Vis spectroscopy for comparison purpose. Table 3 shows the concentrations of particulate iron for five consecutive days, depending on average 8 h exposure of the workers. Each sample reading from both μ-PAD and UV-Vis showed almost the same result and thus we can employ μ-PADs device for the analysis of trace levels of particulate iron in welding fumes without the need of sophisticated analytical methods.

Table 3. Concentration of particulate iron measured from 10 mm filter punch.

| Day | Measured values of $Fe^{3+}$ (mg/L) ± SD from 10 mm punch (n = 3) | | | |
|---|---|---|---|---|
| | μ-PAD | | UV-Vis | |
| | Site 1 | Site 2 | Site 1 | Site 2 |
| 1 | 37.65 ±0.014 | 85.65±0.022 | 38.03±0.017 | 86.11±0.011 |
| 2 | 56.60±0.008 | 45.65±0.015 | 55.86±0.014 | 45.66±0.009 |
| 3 | 36.80±0.024 | 54.52±0.014 | 37.55±0.011 | 54.30±0.009 |
| 4 | 80.71±0.019 | 109.49±0.008 | 83.25±0.011 | 111.17±0.005 |
| 5 | 106.01±0.010 | 80.80±0.003 | 108.13±0.006 | 81.05±0.005 |
| Average | 63.55 | 75.22 | 64.56 | 75.66 |

Site 1 = Gurara, Site 2 = Akaki Kaliti.

As shown above, the results obtained from the μ-PAD measurement ranges from 36.8 – 109.49 mg/L. The average concentration of the two sites also reveals that particulate iron is prevalent. Though, workers at the second welding site are more vulnerable to high concentrations of particulate iron than workers at the first working site. Because the time weighted average (TWA) for an 8 h workday concentration of the metal exceeds the PEL for iron (6 mg/L) set by the OSHA [14], workers in both areas must take precautionary measures. Welder's lung is a pulmonary disease caused by inhaling welding fumes. A recent study on welders discovered that welders who are exposed to fumes for an extended period of time can develop severe liver iron overload [46]. In conclusion, occupational exposure is more likely to be continuous or prolonged, potentially increasing the risk of chronic health conditions.

## CONCLUSION

In this study we proposed and demonstrated a simple and affordable wax-screen printing μ-PAD fabrication approach for the determination of particulate iron from a welding fume. The proposed paper-based sensor demonstrated highly selective and sensitive detection of $Fe^{3+}$ with good linearity and low limits of detection. Hence, the proposed paper-based device can serve as a promising tool for point-of-use application in resource limiting regions especially dealing with iron particulate contamination. The incorporation of two pretreatment zones, the control of surrounding light interference, and the use of a multivariate approach for optimizing experimental parameters all contribute to the device's improved sensitivity for particulate iron analysis. The results from the real sample analysis informed us that there should be an immediate action to be taken by the welders and the concerned body due to the alarming levels of particulate iron found within the welding fume to keep the environment and also the workers' health safe.

## ACKNOWLEDGEMENTS

The authors would like to thank Addis Ababa University Thematic Research Fund and Research Training Fellowship for Developing Countries' scientists (RTF-DCS) scheme of Department of Science & Technology (Government of India) for supporting the project entitled "Developing Innovative Microfluidic Paper-Based Analytical Devices (μ-PADs): Viable solution for Environmental Monitoring in Ethiopia" at the Centre for Environmental Science.

## REFERENCES

1. Ahluwalia, S.S.; Goyal, D. Microbial and plant derived biomass for removal of heavy metals from wastewater. *Bioresour. Technol.* **2007**, 98, 2243-2257.
2. Cain, J.; Fletcher, R. Diagnosing metal fume fever-an integrated approach. *Occup. Med.* **2010**, 60, 398-400.
3. Jomova, K.; Valko, M. Advances in metal-induced oxidative stress and human disease. Toxicol. **2011**, 283, 65-87.
4. Zeidler-Erdely, P.C.; Battelli, L.A.; Salmen-Muniz, R.; Li, Z.; Erdely, A.; Kashon, M.L.; Simeonova, P.P.; Antonini, J.M. Lung tumor production and tissue metal distribution after exposure to manual metal ARC–stainless steel welding fume in A/J and C57BL/6J mice. *J. Toxicol. Environ. Health Part A* **2011**, 74, 728-736.
5. Hoffmeyer, F.; Raulf-Heimsoth, M.; Weiss, T.; Lehnert, M.; Gawrych, K.; Kendzia, B.; Harth, V.; Henry, J.; Pesch, B.; Brüning, T. Relation between biomarkers in exhaled breath condensate and internal exposure to metals from gas metal arc welding. *J. Breath Res.* **2012**, 6, 027105.

6. Della Torre, F.; Cassani, L.; Segale, M.; Scarpazza, G.; Pietra, R.; Sabbioni, E. Trace metal lung disease: A new fatal case of hard metal pneumoconiosis. *Sci. Total Environ.* **1994**, 150, 223.
7. Martinez, A.W.; Phillips, S.T.; Whitesides, G.M.; Carrilho, E. Diagnostics for the developing world: Microfluidic paper-based analytical devices. *Anal. Chem.* **2010**, 82, 3-10.
8. Gavett, S.H.; Koren, H.S. The role of particulate matter in exacerbation of atopic asthma. *Int. Arch. Allergy Immunol.* **2001**, 124, 109-112.
9. Ibfelt, E.; Bonde, J.P.; Hansen, J. Exposure to metal welding fume particles and risk for cardiovascular disease in Denmark: A prospective cohort study. *Occup. Environ. Med.* **2010**, 67, 772-777.
10. Szram, J.; Schofield, S.J.; Cosgrove, M.P.; Cullinan, P. Welding, longitudinal lung function decline and chronic respiratory symptoms: a systematic review of cohort studies. *Eur. Respir. J.* **2013**, 42, 1186-1193.
11. Mehta, S.; Shende, R.; Sampat, B. A rare cause of respiratory distress. *Chest* **2012**, 142, 1002A.
12. Kunimasa, K.; Arita, M.; Tachibana, H.; Tsubouchi, K.; Konishi, S.; Korogi, Y.; Nishiyama, A.; Ishida, T. Chemical pneumonitis and acute lung injury caused by inhalation of nickel fumes. *Intern. Med.* **2011**, 50, 2035-2038.
13. Cate, D.M.; Nanthasurasak, P.; Riwkulkajorn, P.; L'Orange, C.; Henry, C.S.; Volckens, J. Rapid detection of transition metals in welding fumes using paper-based analytical devices. *Ann. Occup. Hyg.* **2014**, 58, 413-423.
14. Kornberg, T.G.; Stueckle, T.A.; Antonini, J.M.; Rojanasakul, Y.; Castranova, V.; Yang, Y.; Rojanasakul, L.W. Potential toxicity and underlying mechanisms associated with pulmonary exposure to iron oxide nanoparticles: conflicting literature and unclear risk. *Nanomater.* **2017**, 7, 307.
15. Anyanwu, B.O.; Ezejiofor, A.N.; Igweze, Z.N.; Orisakwe, O.E. Heavy metal mixture exposure and effects in developing nations: an update. *Toxics* **2018**, 6, 65.
16. Fairbrother, A.; Wenstel, R.; Sappington, K.; Wood, W. Framework for metals risk assessment. *Ecotoxicol. Environ. Saf.* **2007**, 68, 145-227.
17. Muhammed, A.; Hussen, A.; Kaneta, T. Microfluidic paper-based analytical devices coupled with coprecipitation enrichment show improved trace analysis of copper ions in water samples. *Anal. Sci.* **2022**, 38, 123-130.
18. Authority, E.E.P. Provisional standards for industrial pollution control in Ethiopia, prepared under the ecologically sustainable industrial development (ESID), EPA/UNIDO, Addis Ababa, **2003**, 10.
19. Takaku, Y.; Hayashi, T.; Ota, I.; Hasegawa, H.; Ueda, S. Determination of trace levels of iron in a seawater sample using isotope dilution/inductively coupled plasma mass spectrometry. *Anal. Sci.* **2004**, 20 1025-1028.
20. Martin, T.; Brockhoff, C.; Creed, J.; Long, S. Determination of metals and trace elements in water and wastes by inductively coupled plasma-atomic emission spectrometry. *Methods Determ. Met. Environ. Samples* **1992**, 33-91.
21. Bashir, W.A. Photometric determination of iron(III). *Microchem. J.* **1981**, 26, 477-480.
22. Cromartie, R.L.; Wardlow, A.; Duncan, G.; McCord, B.R. Development of a microfluidic device (μPADs) for forensic serological analysis. *Anal. Methods* **2019**, 11, 587-595.
23. Cui, P.; Wang, S. Application of microfluidic chip technology in pharmaceutical analysis: A review. *J. Pharm. Anal.* **2019**, 9, 238-247.
24. Juang, Y.J.; Chang, J.S. Applications of microfluidics in microalgae biotechnology: A review. *Biotechnol. J.* **2016**, 11, 327-335.
25. Lin, Q.; Wen, D.; Wu, J.; Liu, L.; Wu, W.; Fang, X.; Kong, J. Microfluidic immunoassays for sensitive and simultaneous detection of IgG/IgM/Antigen of SARS-CoV-2 within 15 min. *Anal. Chem.* **2020**, 92, 9454-9458.
26. Niculescu, A.G.; Chircov, C.; Bîrcă, A.C.; Grumezescu, A.M. Fabrication and applications of microfluidic devices: A review. *Int. J. Mol. Sci.* **2021**, 22, 2011.

27. Yew, M.; Ren, Y.; Koh, K.S.; Sun, C.; Snape, C. A review of state-of-the-art microfluidic technologies for environmental applications: detection and remediation. *Global Challenges* **2019**, 3, 1800060.
28. Zhang, Q.; Austin, R.H. Applications of microfluidics in stem cell biology. *BioNanoScience* **2012**, 2, 277-286.
29. Abdulsattar, J.O.; Hadi, H. Paper microfluidic device and spectrophotometry methods for colorimetric detection of phenylephrine hydrochloride in pure and pharmaceutical preparations. *Bull. Chem. Soc. Ethiop.* **2022**, 36, 727-736.
30. Asano, H.; Shiraishi, Y. Development of paper-based microfluidic analytical device for iron assay using photomask printed with 3D printer for fabrication of hydrophilic and hydrophobic zones on paper by photolithography. *Anal. Chim. Acta* **2015**, 883, 55-60.
31. Cate, D.M.; Noblitt, S.D.; Volckens, J.; Henry, C.S. Multiplexed paper analytical device for quantification of metals using distance-based detection. *Lab on a Chip* **2015**, 15, 2808-2818.
32. Mentele, M.M.; Cunningham, J.; Koehler, K.; Volckens, J.; Henry, C.S. Microfluidic paper-based analytical device for particulate metals. *Anal. Chem.* **2012**, 84, 4474-4480.
33. Ogawa, K.; Kaneta, T. Determination of iron ion in the water of a natural hot spring using microfluidic paper-based analytical devices. *Anal. Sci.* **2016**, 32, 31-34.
34. Rattanarat, P.; Dungchai, W.; Cate, D.; Volckens, J.; Chailapakul, O.; Henry, C.S. Multilayer paper-based device for colorimetric and electrochemical quantification of metals. *Anal. Chem.* **2014**, 86, 3555-3562.
35. Kamnoet, P.; Aeungmaitrepirom, W.; Menger, R.F.; Henry, C.S. Highly selective simultaneous determination of Cu(II), Co(II), Ni(II), Hg(II), and Mn(II) in water samples using microfluidic paper-based analytical devices. *Analyst* **2021**, 146, 2229-2239.
36. Tesfaye, T.; Hussen, A. Microfluidic paper-based analytical device (μPAD) fabricated by wax screen printing technique for the determination of nitrite and nitrate ion in water samples. *Microfluid. Nanofluidics* **2022**, 26, 22.
37. Baskan, M.B.; Pala, A. A statistical experiment design approach for arsenic removal by coagulation process using aluminum sulfate. *Desalination* **2010**, 254, 42-48.
38. Vincent, J.H.; Ramachandran, G.; Thomassen, Y.; Keeler, G.J. Application of recent advances in aerosol sampling science towards the development of improved sampling devices: the way ahead. *J. Environ. Monit.* **1999**, 1, 285-292.
39. Förch, R.; Schönherr, H.; Jenkins, A.T.A. *Surface Design: Applications in Bioscience and Nanotechnology*, John Wiley & Sons: New York; **2009**.
40. Kannangara, D.; Zhang, H.; Shen, W. Liquid–paper interactions during liquid drop impact and recoil on paper surfaces. *Colloids Surf. A: Physicochem. Eng.* **2006**, 280, 203-215.
41. Pambi, R.; Musonge, P. Application of response surface methodology (RSM) in the treatment of final effluent from the sugar industry using Chitosan. *WIT Trans. Ecol. Environ.* **2016**, 209, 209-219.
42. Pandey, A.; Gupta, A.; Sunny, A.; Kumar, S.; Srivastava, S. Multi-objective optimization of media components for improved algae biomass, fatty acid and starch biosynthesis from Scenedesmus sp. ASK22 using desirability function approach. *Renewable Energy* **2020**, 150, 476-486.
43. Sarrai, A.E.; Hanini, S.; Merzouk, N.K.; Tassalit, D.; Szabó, T.; Hernádi, K.; Nagy, L. Using central composite experimental design to optimize the degradation of tylosin from aqueous solution by photo-fenton reaction. *Materials* **2016**, 9, 428.
44. Behera, S.K.; Meena, H.; Chakraborty, S.; Meikap, B.C. Application of response surface methodology (RSM) for optimization of leaching parameters for ash reduction from low-grade coal. *Int. J. Min. Sci. Technol.* **2018**, 28, 621-629.
45. Miller, J.; Miller, J.C. *Statistics and Chemometrics for Analytical Chemistry*, Pearson Education: England; **2018**.
46. Mariani, R.; Pelucchi, S.; Paolini, V.; Belingheri, M.; di Gennaro, F.; Faverio, P.; Riva, M.; Pesci, A.; Piperno, A. Prolonged exposure to welding fumes as a novel cause of systemic iron overload. *Liver Int.* **2021**, 41, 1600-1607.